

Influence of nanoscale Cu precipitates in α -Fe on dislocation core structure and strengthening

Zhengzheng Chen and Nicholas Kioussis

Department of Physics, California State University, Northridge, California 91330-8268, USA

Nasr Ghoniem

Department of Mechanical and Aerospace Engineering, University of California, Los Angeles, California 90095-1597, USA

(Received 1 May 2009; revised manuscript received 29 July 2009; published 11 November 2009)

Atomistic simulations of the interaction of a screw dislocation in α -Fe with different size bcc Cu precipitates suggest two plausible strengthening mechanisms. For precipitate diameters in the range $1.5 \text{ nm} \leq d \leq 3.3 \text{ nm}$, the dislocation core structure within the Cu precipitate undergoes a polarized to nonpolarized transformation, leading to the dislocation pinning at the precipitate-matrix interface and the bowing out of the dislocation line. The calculated bow-out angle and resolved shear stress required to detach the dislocation from the precipitate are in agreement with recent experiments. The structural transition of larger ($d \geq 3.3 \text{ nm}$) Cu precipitates under high shear stress is responsible for the loss of slip systems and hence for dislocation pinning.

DOI: [10.1103/PhysRevB.80.184104](https://doi.org/10.1103/PhysRevB.80.184104)

PACS number(s): 61.72.Lk, 62.20.F–

I. INTRODUCTION

Neutron and proton irradiation cause hardening and embrittlement in ferritic steels serving as reactor pressure vessels (RPVs). One of the main reasons for the irradiation-induced hardening is the nucleation and growth of Cu precipitates.^{1,2} Because of the low solubility of Cu in Fe at low temperatures, Cu-rich precipitates can easily nucleate and grow under thermal aging. Although Cu precipitates have different crystal structures depending on their size (bcc structure for diameters smaller than about 4 nm and fcc structure for larger diameters), small coherent bcc precipitates are responsible for the strengthening of the RPV steel, serving as obstacles to dislocation motion. Although numerous experimental and theoretical studies have been carried out for Cu particles within the ferrite matrix, the underlying mechanism of dislocation-precipitate interaction and hence the strengthening mechanism are still under investigation. Thus, an understanding of the strengthening mechanism is essential to the prediction, estimation, and extension of the operational life of RPV steels.

The conventional interpretation of the strengthening mechanism, originally proposed by Russell and Brown (RB),³ attributes the effect to the lower shear modulus of Cu precipitates compared to that of the α -Fe matrix. As a result, dislocations can cut and pass through the Cu precipitates. The main difficulty of the RB model, first pointed out by Harry and Bacon,⁴ is that the value of the shear modulus of fcc Cu cannot be used directly for small precipitates, because they have bcc structure which is coherent with the matrix. Osetsyky *et al.*⁵ found that the critical resolved shear stress calculated from the RB model differs significantly from the results of atomistic simulations for small Cu precipitates. An inherent drawback of the RB model is that it is based on continuum elasticity theory, which in turn neglects the important effect of the atomic and electronic structures of the Fe-Cu interface on the dislocation core.

The zero-temperature atomistic simulations of Harry and Bacon⁴ also revealed that a straight screw dislocation near or through spherical precipitates can induce partial transformation of the Cu to a more stable fcc-type structure and thereby

pin the dislocation. Experimental evidence of the transformation of small Cu-rich precipitate (diameter $d \sim 4 \text{ nm}$) from the bcc to the 9R phase in a thermally aged binary Fe-1.3 wt % Cu alloy was found by Lozano-Perez *et al.*⁶ employing transmission electron microscopy (TEM) measurements. The recent molecular-dynamic (MD) simulations of Shim *et al.*⁷ showed the appearance of Orowan loops due to the martensitic structural transformation of the Cu precipitate, which in turn prevents the penetration of the dislocation through the precipitate.

Interestingly, the recent *in situ* TEM experiments of Nogiwa *et al.*^{8,9} showed that dislocations are curved and pinned even by ultrafine Cu precipitates with $d \approx 2 \text{ nm}$. To date, the phase transformation of such small precipitates has not been observed. The critical bow-out angle, θ_c , of dislocations (the angle between two tangent lines drawn from the cusp in the line tension approximation) was found to be obtuse. However, in contrast to the TEM experiment of Lozano-Perez *et al.*⁶ and the MD simulations,⁷ no dislocation loops were observed. This controversy between the theoretical and experimental studies indicates that the underlying atomic origin of the strengthening mechanism by ultrafine Cu precipitates in Fe remains unresolved.

In this paper, we have carried out MD simulations to study the interaction between a $\langle 111 \rangle a/2$ screw dislocation and bcc Cu precipitates of different sizes at low temperature. The rest of the paper is organized as follows: Sec. II describes the method and the computational details. Numerical results for the effect of precipitate size on the dislocation core are presented in Sec. III. Finally, conclusions are summarized in Sec. IV.

II. METHODOLOGY

The MD simulations are performed using the LAMMPS code,¹⁰ with the recent Finnis-Sinclair (FS) Ackland *et al.* (2004) (Ref. 11) interatomic potential for Fe, and the FS potential Ackland *et al.* (1997) (Ref. 12) potentials for Fe-Cu and Cu-Cu. The size of the system, shown schematically in Fig. 1, is $12.2 \times 28.0 \times 19.9 \text{ nm}^3$ along the $X([10\bar{1}])$,

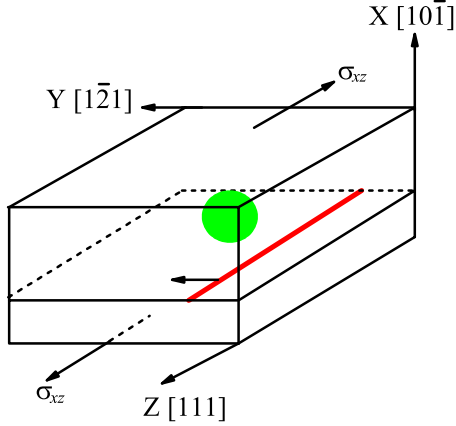


FIG. 1. (Color online) Schematic geometry for the Cu precipitate denoted by green (light gray) interacting with the dislocation line denoted by red (dark gray) placed in the Fe host, where σ_{xz} is the external applied stress.

$Y[1\bar{2}1]$, and $Z[111]$ directions, respectively, containing 576 000 atoms. Periodic boundary conditions (PBC) are applied along the Z direction, while fixed boundary condition (FBC) are employed along both the X and Y directions.¹³ We have considered three bcc Cu precipitates with diameter, d , of 4.4, 2.3, and 1.0 nm, respectively, where the precipitate center is placed at the center of the simulation box. A screw dislocation with Burgers vector $\vec{b}=\langle 111 \rangle a/2$ is placed initially 7.0 nm away from the precipitate center. The molecular-dynamics simulations employ the canonical ensemble with the Noé-Hoover thermostat¹⁴ to keep the temperature constant. The system is first thermally equilibrated at 5 K for 45 ps, and subsequently the external stress, σ_{xz} , is applied on the dislocation, as shown in Fig. 1, with a strain rate of $4 \times 10^7 \text{ s}^{-1}$. The time step throughout the simulation is 1 fs, and the simulation continues till the dislocation detaches from the Cu precipitate. The external stress is applied by displacing equally the atoms in the outermost $(10\bar{1})$ and $(\bar{1}01)$ planes along the $[\bar{1}\bar{1}\bar{1}]$ and $[111]$ directions, respectively. The corresponding shear stress, σ_{xz} , is calculated as the component of the area-averaged force on the surfaces parallel to the Burgers vector.

In order to verify the reliability of FBC along the glide direction, we have carried static calculations of the core structure and Peierls stress, σ_p , for α -Fe, using both the Ackland *et al.* (1997) and Ackland *et al.* (2004) potentials. The former potential gives a degenerate core structure and $\sigma_p=950 \text{ MPa}$ in agreement with previous atomistic simulations¹⁵ employing PBC. On the other hand, the latter Ackland (2004) potential, employed in this work, gives a nondegenerate core in agreement with *ab initio* calculations^{16,17} and $\sigma_p=1.15 \text{ GPa}$ in agreement with that of 1.22 GPa obtained by atomistic simulations¹⁸ using the recently developed Mendeleev¹⁹ potential for α -Fe and FBC.

The presence of surfaces in the FBC introduces image forces²⁰ which, depending on the dislocation position within the simulation box, may affect the dislocation motion. Thus, the image forces need to be corrected, especially when the dislocation is close to the boundary of the simulation box.

The image force within continuum elasticity theory is given by²¹

$$F_{\text{img}} = -\frac{\mu b^2}{4\pi} \left(\frac{1}{d_1} - \frac{1}{d_2} \right), \quad (1)$$

where $\mu=66.9 \text{ GPa}$ is the shear modulus of Fe calculated using the Ackland (2004) potential, b is the magnitude of the Burgers vector, and d_1 and d_2 are the distances of the dislocation from the two surfaces, respectively. When the dislocation is close to the precipitate center, the image forces almost cancel out. The external driving force per unit length can be calculated in terms of the external shear stress tensor, σ , from the Peach-Koehler expression, $F_{\text{dri}}=(\vec{b} \cdot \sigma) \times \vec{t}$, where \vec{t} is a unit-vector tangent to the dislocation line. For a 700 MPa external shear stress, for example, $F_{\text{dri}}=0.18 \text{ N/m}$ compared to $F_{\text{img}} \approx 0.03 \text{ N/m}$ when the dislocation is close to the boundary of the simulation box, i.e., about 16% of the applied stress. Thus, the effective shear stress on the dislocation at the beginning of the simulation box ($d_1=7 \text{ nm}$ and $d_2=21 \text{ nm}$) is about 600 MPa. On the other hand, $F_{\text{img}} \approx 0.02 F_{\text{dri}}$ when the dislocation is 2 nm away from the simulation box center. The image force leads to an acceleration of the dislocation when it reaches the boundary of the simulation box.

In order to determine the position of the dislocation center, we employ the ‘‘centrosymmetry parameter’’ (CSP) visualization approach,²² where the CSP represents a measure of the defective environment in the crystal, i.e., select the atoms according to the amount of displacement relative to their defect-free positions. The differential displacement (DD) map²³ is used to visualize the dislocation core, where the arrows indicate the relative $\langle 111 \rangle$ displacement of neighboring atoms of the dislocation. The length and direction of the arrow denote the magnitude and sign of the displacement difference, respectively. When the arrow touches the centers of the two atoms, their relative displacement is $b/3$.

III. RESULTS AND DISCUSSION

A. 1.0 nm Cu precipitate

Figure 2 shows three MD snapshots of the interaction of the screw dislocation with the 1.0 nm Cu precipitate, as the dislocation glides on the $(10\bar{1})$ plane along the $[\bar{1}\bar{2}1]$ direction under an external stress of 700 MPa. The CSP approach is used to display the Fe core and Cu atoms. The high dislocation average velocity, of $v=120 \text{ m/s}$, as in pure α -Fe, is due to the high strain rate²⁴ and is comparable with the previous MD value of 170 m/s reported by Shim *et al.*⁷ Figure 2(b) shows the configuration when the dislocation intersects the precipitates. We find that under the extreme conditions of MD simulations (very high stress, extremely high strain rates, and low temperatures) the dislocation cuts through the 1.0 nm Cu precipitate without any pinning. However, caution must be exercised in extrapolating MD results to realistic RPV conditions. Due to the spatially dependent image force discussed in Sec. II, the velocity of the dislocation increases as it approaches the precipitate.

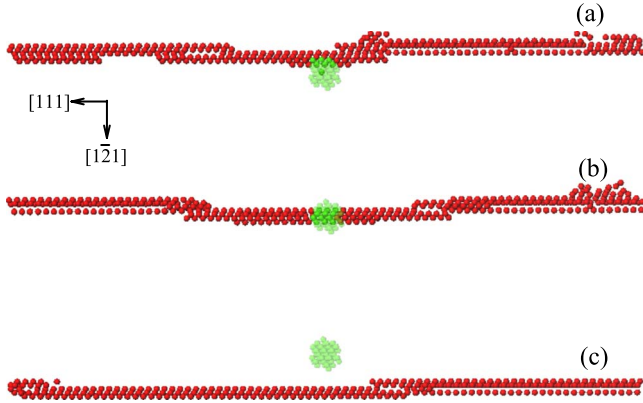


FIG. 2. (Color online) MD snapshots of the dislocation core interacting with the 1.0 nm Cu precipitate as the dislocation glides on the $(10\bar{1})$ plane along the $[1\bar{2}1]$ direction under an external stress of 700 MPa at (a) 268 ps, (b) 274 ps, and (c) 290 ps, respectively. Green (light gray) and red (dark gray) circles represent Cu and Fe atoms, respectively.

B. 2.3 nm Cu precipitate

Figure 3 displays MD snapshots of the screw dislocation interacting with the 2.3 nm Cu precipitate, as the dislocation glides on the $(10\bar{1})$ plane along the $[1\bar{2}1]$ direction under an external stress of 700 MPa. Under this stress, as shown in Figs. 3(a) and 3(b), the dislocation can penetrate into the Cu precipitate, without forming an Orowan loop. The dislocation velocity inside the precipitate decreases to 80 m/s, because the empirical potential employed gives a slightly higher shear modulus for bcc Cu.⁴ As in pure α -Fe, the dislocation glides via nucleation and migration of kink pairs, and the dislocation line remains straight. Under this stress, the dislocation becomes pinned as it approaches the opposite precipitate-matrix interface [Fig. 3(b)], and hence is unable

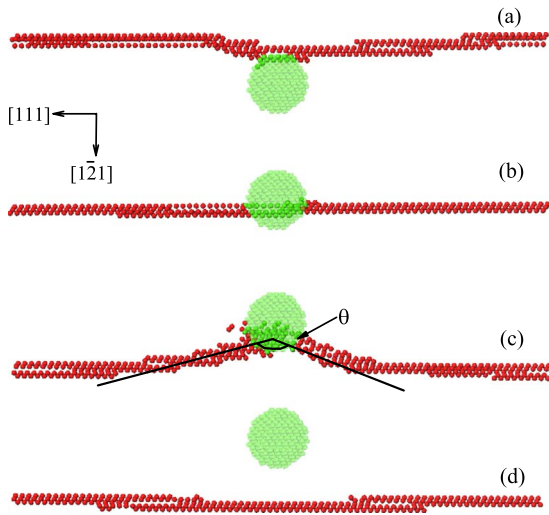


FIG. 3. (Color online) MD snapshots of the dislocation core interacting with the 2.3 nm Cu precipitate as the dislocation glides on the $(10\bar{1})$ plane along the $[1\bar{2}1]$ direction at (a) 243 ps, (b) 272 ps, (c) 312 ps, and (d) 320 ps, respectively. Green (light gray) and red (dark gray) circles represent Cu and Fe atoms, respectively.

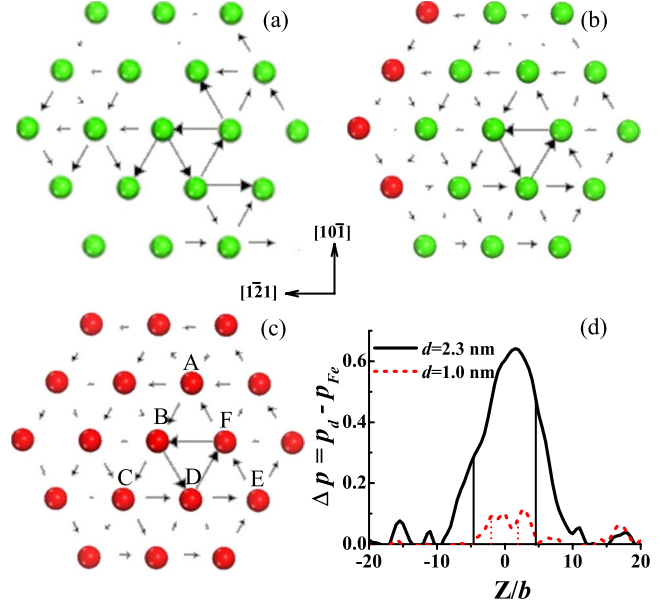


FIG. 4. (Color online) DD maps for the dislocation core inside a Cu precipitate with (a) $d=2.3$ nm; (b) $d=1.0$ nm; and (c) $d=0.0$ nm (pure α -Fe). The red (dark gray) and green (light gray) circles represent Fe and Cu atoms, respectively. (d) Change in dislocation core polarization versus atomic position [normalized to (b)] along the dislocation line. The black solid and red (dark gray) dashed curves correspond to the 2.3 and 1.0 nm Cu precipitates, respectively. The vertical dashed lines indicate the precipitate-matrix interface.

to glide outside the precipitate. Upon increasing the external stress, the dislocation line outside the precipitate continues to glide forward while the short dislocation line segments within the precipitate remains pinned, resulting to a bowing out of the dislocation. The bow-out angle, θ gradually decreases upon increasing the external stress (or equivalently the bow-out curvature increases), from 180° at $\sigma = 700$ MPa until it reaches the critical value of $\theta_c = 144^\circ$ under 1,000 MPa shear stress, where the dislocation suddenly detaches from the Cu precipitate and the dislocation line renders straight.

The dislocation core structure inside the precipitate, for the 1.0 and 2.3 nm precipitates are shown in Figs. 4(a) and 4(b), respectively. For comparison we also display in Fig. 4(c) the core structure in pure α -Fe. The 2.3 nm Cu precipitate changes dramatically the core structure: the displacement field spreads only on three $\{110\}$ semi-infinite planes. In sharp contrast, the 1.0 nm Cu precipitate does not change the core structure. In order to describe the character of the dislocation more quantitatively, we have calculated the core polarization p ,²⁵

$$p = \frac{|\Delta_{AB} - \Delta_{BC}| + |\Delta_{CD} - \Delta_{DE}| + |\Delta_{EF} - \Delta_{FA}|}{b}, \quad (2)$$

where $\Delta_{i,j}$ ($i, j=A, \dots, F$) is the relative displacement between two neighboring atoms in the two columns denoted as i and j in Fig. 4(c). The $p=0$ and 1 cases correspond to the nonpolarized and fully polarized cores, respectively.

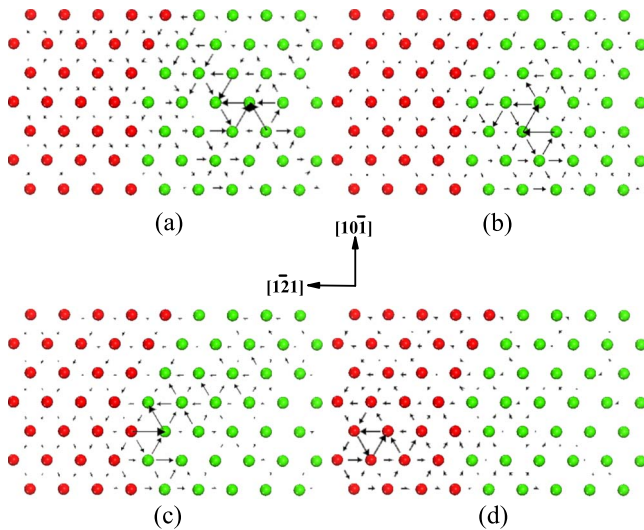


FIG. 5. (Color online) DD maps of the dislocation core of the 2.3 nm Cu precipitate during the detachment process in Fig. 3(c) at (a) 280 ps, (b) 297 ps, (c) 303 ps, and (d) 315 ps. The red (dark gray) and green (light gray) circles represent Fe and Cu atoms, respectively. The dislocation glides along the $[1\bar{2}1]$ direction under an external stress of 1,000 MPa.

In Fig. 4(d) we present the change in core polarization with respect to that of pure α -Fe along the dislocation line. The results clearly show that the change in core polarization is small for the 1.0 nm precipitate, while it is large for the 2.3 nm precipitate and extends beyond the actual precipitate, i.e., the Fe atoms within a shell of about 3 nm around the precipitate acquire a substantial amount of polarization. Figure 4 also shows that the core polarization is well defined in small bcc Cu precipitates, in contrast to the larger bcc Cu precipitates, where the dislocation core spreads out.⁴

In order to analyze the pinning process in more detail, we plot in Fig. 5 the DD map within and outside the 2.3 nm precipitate at different MD snapshots during the detachment process shown in Figs. 3(c) and 3(d). The dislocation glides on the $(10\bar{1})$ plane along the $[1\bar{2}1]$ direction shown in the figure. Although the screw dislocation is gliding under the external stress, the nonplanar core structure, and hence the polarization, are well defined when the dislocation center is at the easy core positions.²⁶ In Fig. 5(a), where the dislocation center is within the precipitate but at a distant from the precipitate/matrix interface, the core is polarized. However, as the dislocation center approaches the interface in Fig. 5(b), it exhibits a split core structure, where the core within the precipitate remains polarized while that slightly farther from the interface begins to transform to a nonpolarized one. In Fig. 5(c), where the dislocation center is at the precipitate/matrix interface, the core becomes nonpolarized with $p \approx 0.25$, similar to the value in pure α -Fe under external stress. Finally, in Fig. 5(d), where the dislocation has detached from the Cu precipitate, the core is rendered to nonpolarized as in pure α -Fe. These results reveal that the dislocation/precipitate detachment process is accompanied with a polarized \rightarrow nonpolarized core transition, which may be responsible for the pinning effect, which is a plausible

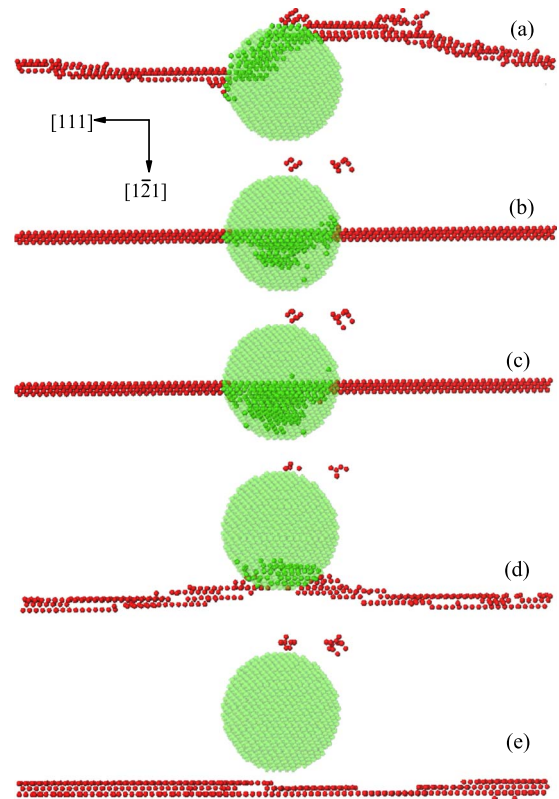


FIG. 6. (Color online) MD snapshots of the dislocation core interacting with the 4.4 nm Cu precipitate as the dislocation initially glides along the $[1\bar{2}1]$ direction, at (a) 260 ps, (b) 330 ps, (c) 540 ps, (d) 722 ps, and (e) 725 ps. Green (light gray) and red (dark gray) circles represent Cu and Fe atoms, respectively.

precipitate-size induced strengthening mechanism, to be discussed in Sec. III D.

C. 4.4 nm Cu precipitate

Figure 6 shows successive MD snapshots of the interaction of the screw dislocation with the larger 4.4 nm Cu precipitate, as the dislocation glides along the $[1\bar{2}1]$ direction. Under the external stress of 700 MPa the dislocation cannot penetrate the precipitate and remains pinned at the precipitate/matrix interface in Fig. 6(a). Upon increasing the stress to 800 MPa [Fig. 6(b)], the dislocation glides further within the precipitate with small fractional segments left at the interface. However, the behavior of the dislocation for the 4.4 nm Cu precipitate is dramatically different from that in smaller precipitates. After reaching the precipitate center under 800 MPa stress, the dislocation stops gliding further within the precipitate upon increasing the external stress. As shown in Fig. 6(c), the part of the Cu precipitate in front of the dislocation begins to transform from its ideal bcc structure with increasing external stress. When the stress reaches a critical value of 2 GPa, the dislocation restarts gliding and it bows out at the precipitate-matrix interface [Fig. 6(d)]. Finally, in Fig. 6(e) the dislocation detaches from the Cu precipitate and the precipitate returns to its bcc structure. Interestingly, the larger precipitate changes also the glide

path of the dislocation. Namely, in contrast to the α -Fe matrix where the dislocation glides on a single $(10\bar{1})$ plane, in the 4.4 nm Cu precipitate it glides alternatively on two $\{110\}$ planes, as pointed out by Ngan and Wen.²⁷ These results suggest that larger Cu precipitates facilitate the activation of secondary slip planes. This Cu-precipitate-induced activation effect was also observed in experiment.⁸

D. Discussion

The core polarization, describing the dislocation core structure, has attracted recently intensive attention. Using four different methods (Finnis-Sinclair potential, ultrasoft pseudopotential DFT, the generalized pseudopotential, and the tight-binding model), Li *et al.*²⁸ demonstrated the lack of correlation between the core polarization and the mobility of dislocations in bcc molybdenum. Rather, this work emphasized the transition from nonplanar to planar core under external stress. Chaussidon *et al.*¹⁸ using two different interatomic potentials for α -Fe found a nondegenerate and degenerate core structure, respectively. The latter potential gave two critical stresses, where when the applied stress reaches the lower critical value the dislocation advances by one atomic distance adopts a metastable configuration and remains fixed until a second upper critical stress is reached, above which the motion becomes unbounded. Similar behavior was also reported in our previous work,²⁹ where Cu nanocolumn precipitates change the dislocation core polarization in Fe and induce a two-step activation process. The results in Sec. III B also suggest that the pinning effect in the 2.3 nm Cu precipitate may be related to the change in dislocation-core polarization. Similar conclusions were also drawn in previous atomistic simulations for bcc metals.^{25,27} Thus, the relationship between the core polarization and dislocation mobility (σ_p) remains unresolved.

The results of Sec. III B suggest that if the Cu precipitate is large enough to change the polarization, the dislocation needs to transform its core structure in order to move out from the precipitate. Thus, the dislocation line begins to bow out to supply the extra force for the transition of the core structure. The presence of a critical precipitate size impeding the dislocation motion has been reported both in experiments^{8,9} and atomistic simulations.^{4,5} We find that the core changes structure at the critical diameter, $d_{cr}=1.5$ nm, in good agreement with the *in situ* TEM experiments of Nogiwa *et al.*,⁸ suggesting that the critical precipitate size may be interpreted as the size where the dislocation core changes its structure.

The increment in critical shear stress, $\Delta\tau_{cr}$, due an obstacle can be expressed in terms of the critical bow-out angle θ_c ,^{30,31}

$$\Delta\tau_{cr} = \frac{\mu b}{L} \left[\cos\left(\frac{\theta_c}{2}\right) \right]^{3/2} \left(\frac{4\pi + a_c}{5\pi} \right), \quad (3)$$

where L is the average distance between neighboring obstacles along the dislocation line and $\mu=66.9$ GPa. Our MD

simulations yield (Fig. 2) $\theta_c=144^\circ$, in good agreement with the average value of 150° reported in the *in situ* TEM observations.^{8,9} Using the MD value of $\theta_c=144^\circ$ and $L=19.9$ nm (dimension of the simulation box) we find that $\Delta\tau_{cr}=137$ MPa.

The precipitate-induced increase in the shear stress, $\Delta\tau_{cr}$, can also be determined using the line-tension approximation.⁴ The detachment of the dislocation from the precipitate occurs when the critical force F_{cr} exceeds the pinning force⁴

$$F_{cr} = \Delta\tau_{cr} L b \geq F_{pin}, \quad (4)$$

where $F_{pin}=2\Gamma \cos(\frac{\theta}{2})$ and $\Gamma=\mu b^2/2$ is the line tension. Using the MD value for $\theta_c=144^\circ$ we find that $F_{pin}=2.05 \times 10^{-9}$ N, yielding $\Delta\tau_{cr}=302$ MPa, in agreement with the theoretical value of 335 MPa for $L=17$ nm in Ref. 4, who employed also the line-tension approximation.

The above results suggest that the change in core polarization may be a plausible strengthening mechanism for precipitates with $1.5 \text{ nm} \leq d \leq 3.3 \text{ nm}$. On the other hand, for larger size precipitates polarization is not a well-defined quantity. The results in Figs. 6(b) and 6(c) reveal massive structural deformation within the precipitate leading to loss of coherency between the precipitate and the matrix,⁷ which in turn impedes dislocation motion.⁴ Thus, for $d \geq 3.3$ nm, the structural transformation becomes important and may be responsible for dislocation pinning. This critical size is in agreement with the value of 3.5 nm reported in the TEM measurements of Lozano-Perez *et al.*⁶ The structural transition may also be responsible for the activation of secondary slip systems in larger Cu precipitates. The asymmetric behavior between the incident and transmitted dislocation in both the 2.3 and 4.4 nm Cu precipitates in Figs. 3 and 6, respectively, may be understood as follows: before the dislocation intersects and/or penetrates, the precipitate is in the perfect bcc structure, while when the dislocation lies within the precipitate, it has already been deformed through the strain field. This asymmetry indicates the importance of the internal and/or residual strain on the precipitate/dislocation interaction.

IV. CONCLUSION

We have carried out MD simulations to study the effect of different size Cu precipitates on the dislocation core structure in α -Fe. The results suggest two different mechanisms depending on the Cu precipitate size. For precipitates with $1.5 \text{ nm} \leq d \leq 3.3 \text{ nm}$, the dislocation core structure changes from polarized to nonpolarized during the detachment process. This transformation results in the pinning of the dislocation at the precipitate-matrix interface. The required extra stress is in turn provided by the bowing out of the dislocation line. The calculated values for both the bow-out angle and the increment of shear stress required to detach the dislocation from the precipitate are consistent to recent TEM

experiments and atomistic simulations. For larger precipitates, with $d \geq 3.3$ nm, the structural transition plays an important role on dislocation motion, in agreement with the TEM measurements of Lozano-Perez *et al.*⁶ Namely, under high shear stress, the larger Cu nanoprecipitate undergoes a structural transition from its ideal bcc structure, thus impeding dislocation motion due to loss of slip systems.

ACKNOWLEDGMENTS

The authors acknowledge valuable discussions with G. Ackland. This research was supported by DOE NERI under Grant No. DE-FC07-06ID14748, NSF-NIRT under Grant No. CMS-0506841, and NSF-PREM under Grant No. DMR-00116566.

-
- ¹J. Buswell, P. Bischler, S. Fenton, A. Ward, and W. Phythian, *J. Nucl. Mater.* **205**, 198 (1993).
²G. R. Odette and G. E. Lucas, *JOM* **53**, 18 (2001).
³K. C. Russell and L. M. Brown, *Acta Metall.* **20**, 969 (1972).
⁴T. Harry and D. Bacon, *Acta Mater.* **50**, 195 (2002); **50**, 209 (2002).
⁵Y. Osetsky, D. Bacon, and V. Mohles, *Philos. Mag.* **83**, 3623 (2003).
⁶S. Lozano-Perez, M. L. Jenkins, and J. M. Titchmarsh, *Philos. Mag. Lett.* **86**, 367 (2006).
⁷J. Shim, Y. Cho, S. Kwon, W. Kim, and B. Wirth, *Appl. Phys. Lett.* **90**, 021906 (2007).
⁸K. Nogiwa, T. Yamamoto, K. Fukumoto, H. Matsui, Y. Nagai, K. Yubuta, and M. Hasegawa, *J. Nucl. Mater.* **307-311**, 946 (2002).
⁹K. Nogiwa, N. Nita, and H. Matsui, *J. Nucl. Mater.* **367-370**, 392 (2007).
¹⁰S. J. Plimpton, *J. Comput. Phys.* **117**, 1 (1995).
¹¹G. Ackland, M. Mendeleev, D. Srolovitz, S. Han, and A. Barashev, *J. Phys.: Condens. Matter* **16**, S2629 (2004).
¹²G. Ackland, D. Bacon, A. Calder, and T. Harry, *Philos. Mag. A* **75**, 713 (1997).
¹³Z. Chen, G. Lu, N. Kioussis, and N. Ghoniem, *Phys. Rev. B* **78**, 134102 (2008).
¹⁴W. G. Hoover, *Phys. Rev. A* **31**, 1695 (1985).
¹⁵J. Marian, W. Cai, and V. Bulatov, *Nature Mater.* **3**, 158 (2004).
¹⁶S. Frederiksen and K. Jacobsen, *Philos. Mag.* **83**, 365 (2003).
¹⁷L. Ventelon and F. Willaime, *J. Comput.-Aided Mater. Des.* **14**, 85 (2007); Emmanuel Clouet, Lisa Ventelon, and F. Willaime, *Phys. Rev. Lett.* **102**, 055502 (2009).
¹⁸J. Chaussidon, M. Fivel, and D. Rodney, *Acta Mater.* **54**, 3407 (2006).
¹⁹M. I. Mendeleev, S. Han, D. J. Srolovitz, G. J. Ackland, D. Y. Sun, and M. Asta, *Philos. Mag.* **83**, 3977 (2003).
²⁰C. Domain and G. Monnet, *Phys. Rev. Lett.* **95**, 215506 (2005).
²¹J. P. Hirth and J. Lothe, *Theory of Dislocations*, 2nd ed. (Wiley, New York, 1982), p. 68.
²²C. L. Kelchner, S. J. Plimpton, and J. C. Hamilton, *Phys. Rev. B* **58**, 11085 (1998).
²³V. Vitek, *Cryst. Lattice Defects* **5**, 1 (1974).
²⁴Y. Osetsky and D. Bacon, *J. Nucl. Mater.* **323**, 268 (2003).
²⁵G. Wang, A. Strachan, T. Cagin, and W. A. Goddard, III, *Mater. Sci. Eng., A* **309-310**, 133 (2001); *Phys. Rev. B* **67**, 140101(R) (2003).
²⁶N. I. Medvedeva, Yu. N. Gornostyrev, and A. J. Freeman, *Phys. Rev. B* **72**, 134107 (2005).
²⁷A. H. W. Ngan and M. Wen, *Phys. Rev. Lett.* **87**, 075505 (2001).
²⁸J. Li, C. Z. Wang, J. P. Chang, W. Cai, V. V. Bulatov, K. M. Ho, and S. Yip, *Phys. Rev. B* **70**, 104113 (2004).
²⁹Z. Chen, N. Kioussis, N. Ghoniem, and T. Hasebe, *Phys. Rev. B* **77**, 014103 (2008).
³⁰A. J. E. Foreman and M. J. Makin, *Philos. Mag.* **14**, 911 (1966).
³¹A. J. E. Foreman and M. J. Makin, *Can. J. Phys.* **45**, 511 (1967).